Comparative catalytic activity of low-cost route prepared TiO_2 and silver nanoparticle modified TiO_2 for visible light assisted dye degradation and mechanism insights

F. M. Al-Zahrani [a] , N.S. Alsaiari [a] , T. Radika [b*], K. M. Abualnaja [c], R. Jothiramalingam[d] , M. Ouladsmane [e]

[a]*Department of Chemistry, College of Science, Princess Nourah bint Abdulrahman University, P. O. Box 84428, Riyadh 11671, Saudi Arabia.*

[b]*C-MET, Center for Materials for Electronics Technology [C-MET], Athani P.O, Thrissur, Kerala, India.*

[c]*Department of Chemistry, College of Science, Taif University, Taif 21944, Saudi Arabia.*

[d]*Department of Chemistry, College of Science, King Saud University, Riyadh, Kingdom of Saudi Arabia.*

[e] *Advanced Materials Research Chair, Chemistry Department, College of Science, King Saud University, Riyadh 11451, Saudi Arabia.*

Pure rutile phase of Titanium dioxide (r-TiO_2) is prepared by nitric acid assisted hydrothermal process. XRD, Ft-IR, Raman spectroscopic techniques were utilized to confirms the formation of pure rutile phase for as prepared titania materials. SEM (scanning electron micrograph) images confirms the formation of Cauliflower like morphology for as prepared R-TiO_2 with reduced particle size below 5 nm. Ag-TiO_2 shows the hexagonal cubic shaped morphology with improved catalytic activity. The catalytic activity of as prepared R-TiO_2 and silver modified TiO_2 have analysed under visible light irradiation for dye degradation reaction. Dye degradation is occurred very effectively even at higher concentration of MB at reduced time intervals from 5 h to 3 hours of reaction time. Hence, the prepared pure Rutile titania and silver modified TiO_2 are shown improved and effective activity in the presence of visible light irradiaiton for dye degradation and discoloration process.

(Received October 10, 2021; Accepted February 28, 2022)

Keywords: Rutile, Catalyst, Dye degradation, Nanoparticle, Titania

1. Introduction

Amorphous form Titanium dioxide or titania (TiO2) has limited photocatalytic applications due to higher degree of defects which promote rapid electron- hole recombination. The three main crystalline forms of TiO2 are; Rutile, Anatase and Brookite.[1–3] Anatase and Rutile are the ones which have been extensively studied since Brookite is rather difficult to isolate and prepare the pure form. Rutile is the most stable phase while Anatase and Brookite are metastable. Among the three phases, Anatase is the most photosensitive form. Hydrothermal method is feasible and perfect crystallization of nanomaterials at high temperation condition with increased pressur condition. [4–6]. A temperature difference is maintained between the opposite ends of the growth chamber.

The advantages of hydrothermal treatment are, nano sized materials can be synthesized with high purity, particle size distribution can maintain almost uniform and Insights into adsorptive interactions between antibiotic molecules and rutile-TiO2 (110) surface Intermolecular interactionsbetween antibiotic molecules, tetracycline (TC), amoxicillin (AX) and ampicillin (AP), and rutile (110) surface were thoroughly studied by density functional theory

* Corresponding author: rads12@gmail.com
https://doi.org/10.15251/JOR.2022.181.101

calculations in soli state. The adhesive property of antibiotic molecules on r-TiO2 surface is large compared to anatase TiO2.[10] Titanium dioxides with nanostrucutres could exist with mixed phase compositions consitst of highest proportion of anatase and rutile phase. Marjo rutile phase containg TiO2 have shown higher photocatalytic activity for 4-Chlorophenol (4-CP) and dye degradation towards water treatment application [11]. In another recentl report revels that the silver doped ruitle phase thin film materials form of titanium dioxide with crystal plan (1 1 0) and (1 1 1). The different amont silver nanoparticle doped with TiO2 synthesized by hydrothermal method without additive agents. [12,13] The flowerlike structures are obtained for silver doped TiO2. The silver nanoparticle with loading capacity of 1 wt% doped TiO2 shown highest methylene blue degradation. The synergistic effect between both (1 1 0) and (1 1 1) facets and Ti3+-oxygen vacancy are the mina factor for the improved activity by reduce the band gap and working as an electron trap [14-15]. The present study demonstrates the preparation of TiO2 and Ag doped TiO2 materials through sol-gel and hydrothermal process followed by characterization of various physicochemical properties. he prepared materials using various physicochemical techniques. The valuation of photosensitive activity of the as-prepared materials has also been studied using Methylene blue dye degradation reactions.

2. Experimental

2.1. Preparation of rutile TiO_2 hydrothermal method

To prepare pure phase of rutile titania, 55 mL of titanium (1V) butoxide was dissolved in 72 mL of isopropanol. Distilled water (15 mL) was added dropwise under vigorous stirring at room temperature. The pH of the mixture was adjusted to ~3, by adding one or two drops of 70 % HNO_3. The mixture was stirred for about 3 h at room temperature. The obtained gel was dried (373 K, 12 h) and calcined at 773 K (3 h). To study the effect of nitric acid concentration, the different molar concentrations of nitric acid added pure TiO_2 have also been prepared. The different molar concentrations of HNO_3 solution (2, - 10 M) to prepare various 2T to 10 T (TiO_2) catalytic materials.

2.2. Preparation of Ag/TiO_2

Ag-doped TiO_2 (Ag/TiO_2) materials were prepared by the sol-gel method. Different mole percentage (0.1, 0.3 and 0.5, Ag mol %) of Ag was prepared by taking corresponding amounts of $AgNO_3$ solution. The metal salt solution was added drop wise under vigorous stirring to a mixture of titanium (1V) butoxide and isopropanol. One or two drops of 70 % HNO_3 were added into it to adjust the pH to ~3. The mixture was stirred for about 3 h at room temperature. The obtained gel was dried overnight (273^0C) and calcined at 773 K (3 h). The different mole ratio of prepared Ag-Titania designated as 0.1 AgT, 0.3AgT, 0.5 AgT, respectively.

2.3. Material characterization

The instrumental techniques used for the characterization of prepared materials are Powder X-ray diffraction, Optical images, DR UV-Visible spectroscopy, FT-IR spectroscopy, Raman spectroscopy, SEM (Scanning electron microscope), and TG-DSC. Here, powder X-ray diffraction studies are carried out using an AXS Bruker D5005 X-ray diffractometer (Germany) with vertical goniometer. X-ray generator was operated at 40 kV and 30 mA, CuKα(λ=1.54Å) radiation with Ni Filter. The Crystalline phases are identified by comparison with the standard JCPDS data file. The BET surface area measurements were carried out at liquid nitrogen temperature on BET surface area analyzer (NOVA 1200, Quantachrome, USA). Degassing of all the samples was carried out at 573K for one hour before the analysis under nitrogen atmosphere. The vibrational modes of the prepared materials were studied using FT-IR spectroscopy (Schimadzu IR spectrometer Japan) over the range 400 - 4000 cm^{-1}.

2.4. Band gap evolution of synthesized Rutile TiO_2

The obtained Diffuse reflectace spectra was converted into to a magnitude proportional to the extinction coefficient (α) through the Kubelka-Munk function (eq.1):

$$F(R) = (1-R)^2 / 2R \quad (1)$$

E_g can also be calculated according to the eq.2:

$$E_g = hc / \lambda = 1240/\lambda \quad (2)$$

where E_g is the band gap energy, h is the Planck's constant, c is the light velocity (m/s), and λ is the wavelength (nm).

2.5. Photocatalytic study of Synthesized Rutile Titania and Ag modified Titania (Ag-TiO_2) catalysts

The 500 cm^3 capacity, cylindrical quartz photoreactor (HEBER SCIENTIFIC, immersion type photoreactor) which was used for the methylene blue degradation study of to exploit the efficiency of the present method prepared catalytic nanomaterials. evaluate the photocatalytic activity of the prepared samples. Approximately 0.05 g of the catalyst was used for the each reaction and the reactant volume maintained with 50 mL of methylene blue aqueous solution in quartz reactor.. Before start the reaction under photocatalytic mode, the reactor was kept in dark for 5 minutes followed by irradiated with Visible lamp (300 W, Visible, 230 V, AC) and circulation of water was maintained throughout the reaction. At various time interaval the dye solution is taken for analysis in UV - Visible spectrophotometer.

3. Results and discussion

3.1. Crystallinity and surface area characterization

Figure 1 shows the XRD pattern of highly crystalline and well-resolved features characteristics peaks corresponding to rutile TiO_2. The XRD pattern obtained is in good agreement with the JCPDS file. It suggests that the phase formation depends on the hydrothermal reaction conditions. The TiO_2 prepared under the hydrothermal conditions preferentially forms rutile phase as major for acid assisted method prepared TiO_2. The pattern obtained for 2T to 10 T samples represents similar peaks (Fig.1a) corresponding to planes of TiO_2 at 2Θ = 27.4 (110), 36.0 (101), 39.1 (200), 41.2 (111), 44.0 (210), 54.3 (211), 56.6 (220), 62.7 (002), 64.0 (310) and 69.0 (301) respectively. The obtained XRD pattern shows pure crystallinity with well-resolved features characteristics of rutile TiO_2 [16]. Fig. 1c shows the reference reported images of Rutile TiO_2 with JCPDS data of 21-1276. Fig.1b shows the Tauc plot of different acid concentrated prepared Rutile TiO_2 by adopting equations 1 and 2, we calculated the band gap values of pure TiO_2 materials.

The Diffuse Reflectance UV–Vis spectrum of pure TiO_2 consist of a broad intense absorption peak at 410 nm (corresponding to band gap of 3.0 eV calculated from the formula from equation (1) and (2)) due to Charge – Transfer from the VB formed by 2p orbitals of the oxide anions (O^{2-}) to the CB formed by 3d t_{2g} orbitals of the Ti^{4+} cations.[17,18]. To find out the bandgap value of as prepared rutile titania nanoparticles, tauc plot was utilized in the present study. To determine optical band gap of the as–prepared nanotubes and nanotubes thermally treated at 250°C for 2h, UV-Visible diffuse reflectance spectra were recorded and converted into tauc plot (Figure 1b, inset). The samples 2T an 4T showed absorption in the UV region. However, the red shift of the absorption edge (i.e. lower energy) was obtained. The reduction in bandgap values is obtained due to the formation of oxygen and hydrogen vacancies thus inducing defect states and reducing the bandgap of titanate nanoparticles (Sun et al., 2015).

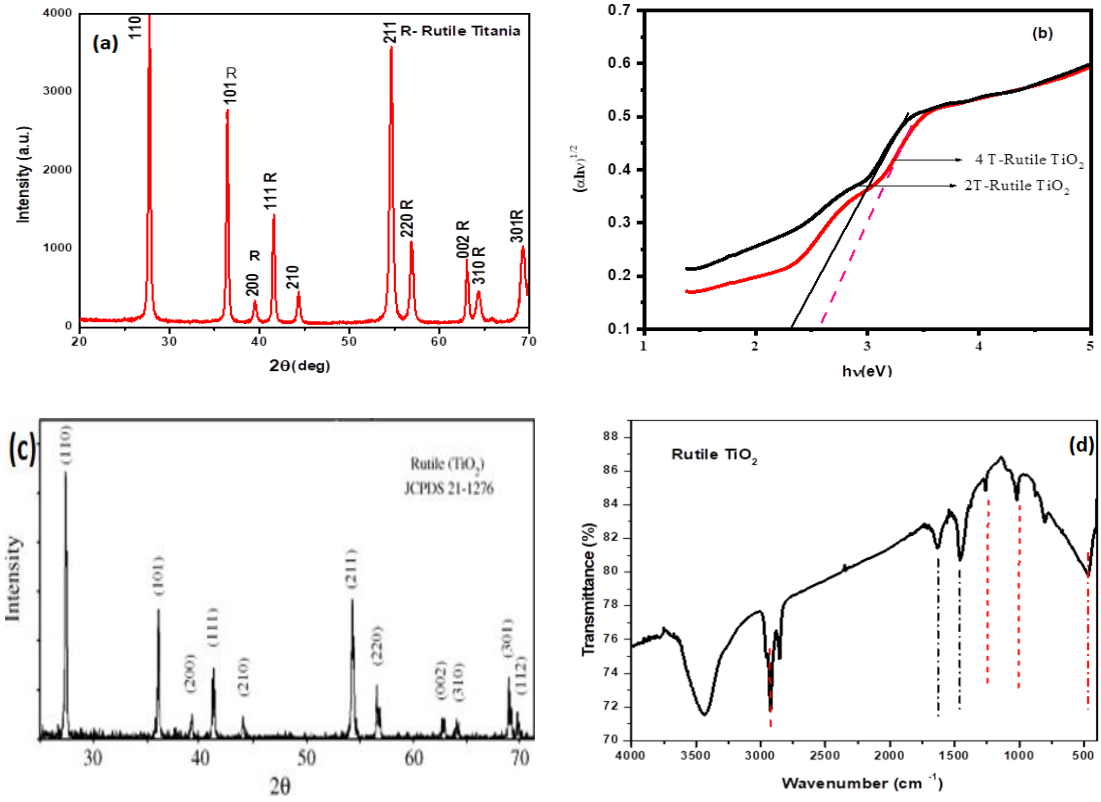

Fig. 1. (a-d) XRD pattern of Concentrated acid treatment and hydrothermal method prepared Rutile TiO_2 (4T).

Table 1. Comparative BET surface are values of the P25 Degussa and Rutile phase TiO_2 materials.

Sl. no.	Material	BET Surface area (m^2/g)	Particle size (nm)
1.	P25	53.6	26.5
2.	TiO_2 (4T)	105.5	14.9
3.	TiO_2 8T	28.3	50.3
4.	TiO_2 6T	13.5	57

The specific surface area of the prepared materials was determined by the Brunauer-Emmette-Teller (BET) method. The BET surface area of hydrothermally prepared pure TiO_2 is 105.5 m^2/g which is higher than 53.6 m^2/g of commercially available titania (P25). The higher surface area is useful in the efficiency of photosensitive activity as it implies larger contact surfaces exposed to the reagents. BET surface area and particle size for the materials prepared under optimum conditions in comparison with Degussa-P25. Table 1 compiles the BET surface area and particle size for the materials prepared through the hydrothermal method in comparison with P25. BET surface area of the hydrothermal prepared TiO_2 is higher (105.5 m^2/g) compared to 8T (28.37 m^2/g) and P25. The high surface area of the prepared samples 8T and 6T is due to the nanosize of the particles. The observed higher surface area of 8T can be due to the smaller particle size. The XRD pattern of silver nanoparticle modified TiO_2 has shown in Fig. 2 and it depicts major rutile phase of Titania existence with anatase phase together. The incorporation of silver nanoparticles in the lattice of titania causes broadening of peaks at 22 ^{o}, 38^{o,} and 49^o. Pattern posses well-resolved feature characteristics of anatase phase with (101), (112), (200) planes and characteristics of rutile phase with (110), (101), (111), (210), (211), (220), (002), (310), (301) planes. The intense peak is corresponding to (112) plane of the anatase phase. It agrees with the

standard values in the JCPDS file [18]. Thus Ag modified TiO_2 consists of both anatase and rutile TiO_2 which forms during the sol-gel preparation due to the presence of acidity solution. Surface area value is another important factor for catalytic surface due to anchoring of incoming molecules. Silver modification causes a decrease in the surface area values gradually concerning the dosage of silver addition into the titania lattice. The measured surface area values and particle size measurement of silver nanoparticle modified titania have shown in Table 2.

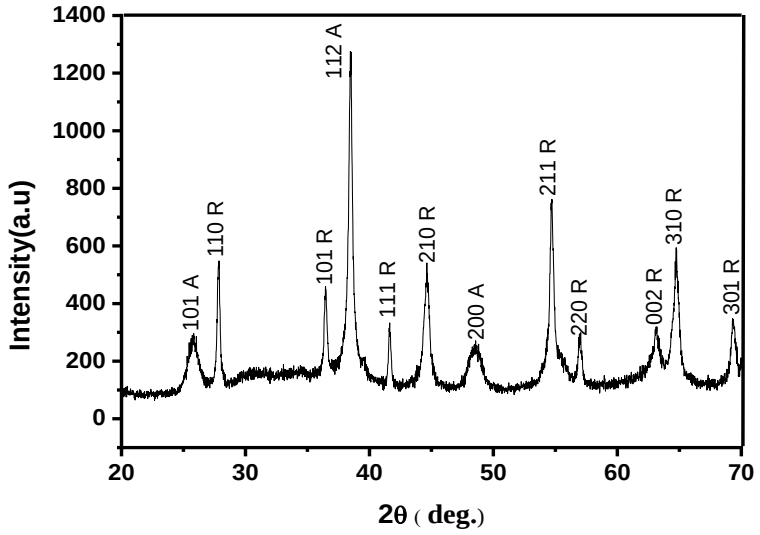

Fig. 2. XRD pattern of Concentrated acid treatment hydrothermal method prepared silver modified Rutile TiO_2.

Table 2. Comparative BET surface area of commercial and silver nano modified TiO_2 materials.

Sl.no	Material	BET Surface area (m^2/g)	Particle Size (nm)
1	Degussa-P25	53.6	26.5
2	TiO_2 (4T)	105.5	14.9
3	0.3 AgT	22.0	71.7
4	0.5 AgT	10.0	157.8

3.2. Morphology and optical property characterization

In order to understand the morphology of the prepared materials, investigation was made using optical microscope. Images of prepared rutile TiO_2 obtained from optical microscope are shown in the following Figures (Fig. 3 (a-c)).

The optical images of 2T and 4T route prepared rutile titania and it appeared as irregular particle and non-uniformity in spherical shapes formation. However, in the case of 6T to 10T images (Fig. 3 a-c) appear more spherical in nature.

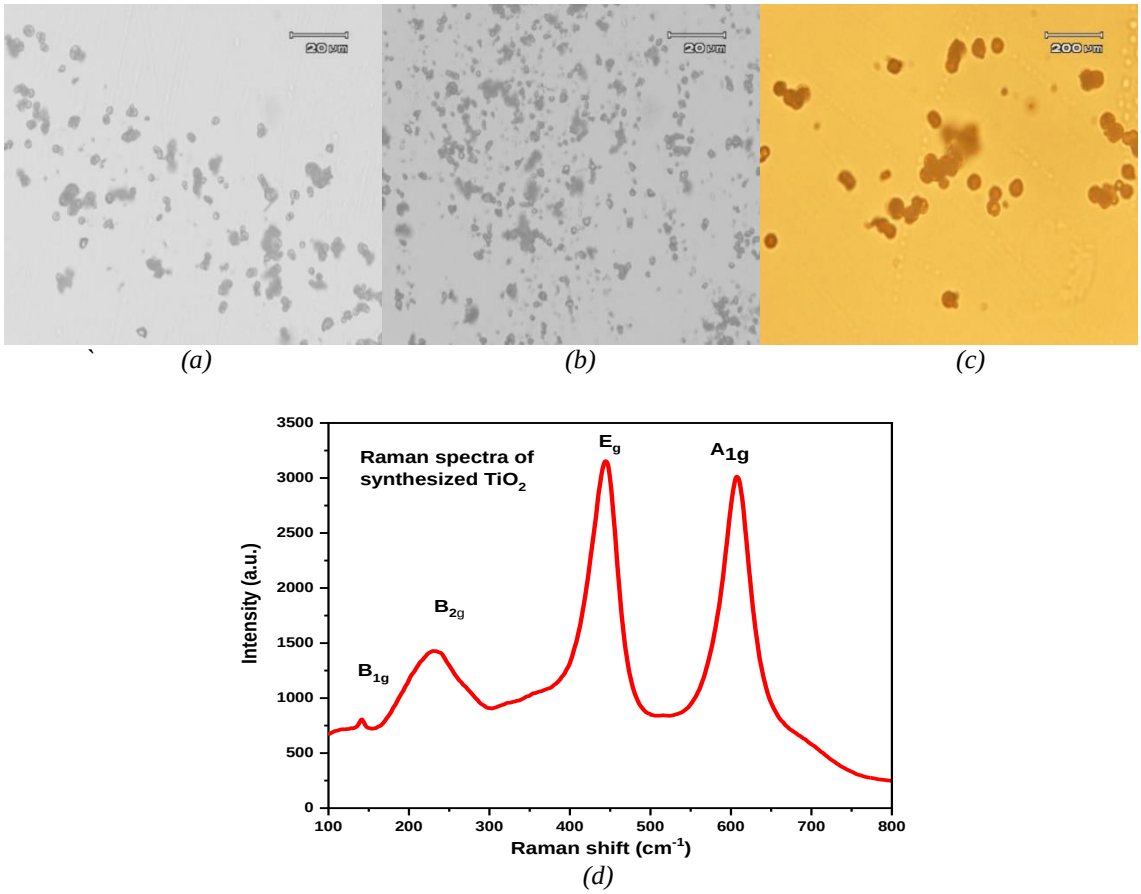

Fig. 3. Optical images of (a) 2T (b) 4T (c) 6T (d) Ramang spectra of TiO_2

Fig. 3d shows the Four Raman active modes with symmetry of A_{1g}, B_{1g}, B_{2g} and E_g have been found for the as-prepared titania sample and were matched with reported data of the rutile TiO_2 at 143 (B_{1g}), 447 (E_g), 612 (A_{1g}), and 826 (B_{2g}) cm^{-1}. [3] In Fig. 3d the two intense peaks at 443 (E_g) and 609 (A_{1g}) cm^{-1} are due to presence of rutile phaseThe Raman peak at 233-234 cm^{-1} is due to the multiple phonon scattering processes, which is characteristic Raman peak of rutile type TiO_2. A small peak at higher Raman-shifts B_{1g} (140 cm^{-1}) has also been observed, which is also in good agreement with the reported Raman features of rutile TiO_2. Raman features of Rutile phase are far less characterized: a redshift attributed to non-stoichiometric effects has been reported for the E_g Rutile mode and a random shift for the Rutile A_{1g} mode. Thus the Raman spectrum confirms the formation of Rutile TiO_2 under the hydrothermal reaction conditions as observed from the powder XRD pattern.

The FT-IR spectrum of as-prepared TiO_2 shows (Figure 1d) band at ~469 cm^{-1}due to Ti-O stretching vibration [19]. The presence of the band at ~1640cm^{-1} suggests the characteristic bonding vibration of the adsorbed water molecule. Furthermore, the bands in the range 3400-2750 cm^{-1} are due to the stretching vibrations of –OH groups. It has been reported that the surface of –OH groups, which are quite polar give strong IR bands in the range 3000-4000 cm^{-1} and 1400-1700 cm^{-1}. The band at 2363 cm^{-1} can be assigned to the CO_2 vibration from the environment. The absence of characteristic peak of -OH groups (1200-1000 cm^{-1}) confirms that the Titanium alkaloids are completely getting hydrolyzed to TiO_2 nanoparticles during calcination [20].

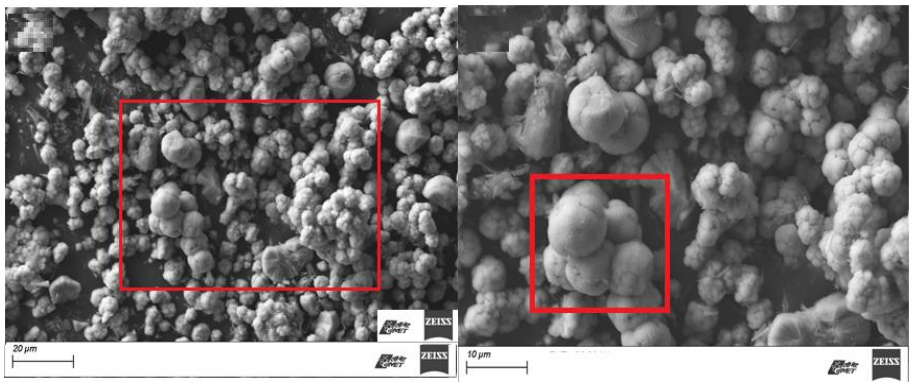

Fig. 4. (a-b) SEM images with different magnifications of Rutile titania (6T) and Rutile titania (4T) prepared by acid-treated hydrothermal method.

Fig. 4 (a-b) shows the SE micrographs of synthesized rutile titania nanoparticles of 6T route acid-treated samples. It shows the group of titania nanoparticles that forms cauli-flower shaped particles that split into individual nanorods of titania (Fig 3b). Fig. 3 (c) shows a magnified image of aggregated particle formation with spherical flower shape existing in a non-uniform manner for 4 T route prepared titania sample compared to higher concentration route (6T) prepared titania. In comparison with literature reports, the cauliflower shape of titania was not reported and the specific structural morphology formation due to acid assisted hydrothermal reaction condition and nitric acid treatment causes such specific structures for as synthesized pure rutile phase of titania sample [21]. Fig. 4 (a-d) shows the SEM images of silver modified Titania samples prepared same methodology of pure titania. Silver addition transforms the particle morphology and its existence with hexagonal rods formation together with spherical particle formation. Figure 4c shows the elemental analysis and elemental identification of silver nanoparticle modified titania sample prepared at 0.3 mole of silver incorporation. EDX spectra clearly show the existence of silver in titania lattice. Silver incorporation causes the aggregation of titania particles and it forms dense flakes followed by the formation of hexagonal cubes for 0.3Ag-TiO_2 materials. Fig. 4d shows the large plates morphology of hexagonal rod-shaped 0.3Ag-TiO_2 at magnified sites.

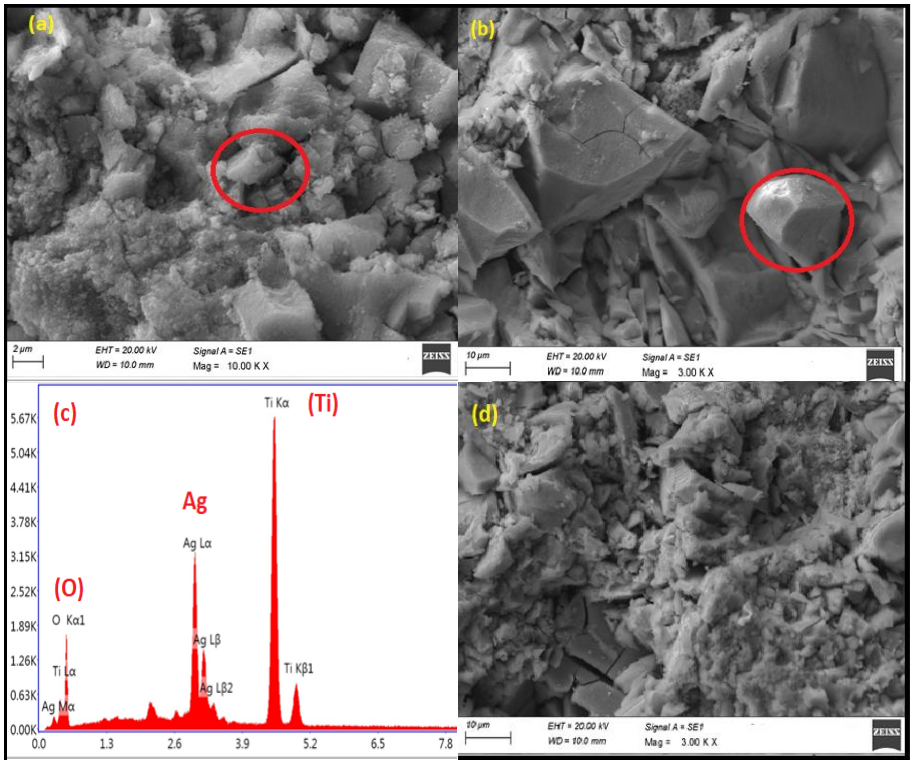

Fig. 5 (a-d) SEM images with different magnifications of silver modified titania and Fig. 4 (c) EDX spectra of Ag-doped titania prepared by acid-treated hydrothermal method (d) Ag-TiO_2 large hexagonal plates at a magnified region.

3.4. Photosensitive property of as prepared Rutile TiO_2 and silver modified TiO_2 materials (Ag-TiO_2)

Figures 6-8 shows the methylene blue (MB) degradation reaction the as-prepared photosensitive materials. The fast degradation of MB occurs due to the effective absorption of visible light and thus reduces the electron-hole recombination. This will enhance the photosensitive property of the prepared titania and silver-modified titania catalysts. [22-23]. All prepared catalysts are showing effective and complete MB degradation followed by discoloration within 4 hours reaction time. Fig: 6-7 shows the UV-Vis spectrum of degradation of MB using various R-TiO_2 (2T, 4 T, and 6T). The presence of visible light causes effective degradation of MB have obtained using 4T and 6 T compared to commercial Degussa P25 titania. Fig: 6 (a-b) shows comparative MB degradation in the presence of commercial titania and 4T rutile titania. Similarly, Fig.7(a-b) shows the degradation patterent of 2T and 6T mateials. In the presence of visible light, degradation of MB using 4T and 6T route prepared titania shown higher degradation compared to 2T and commercial titania. The improved performance is due to different particle sizes, surface area values, active site's existence, and morphology of prepared titania materials. Thus, the morphology of the TiO_2 has also played an important role in the photosensitive activity. In the presence of prepared samples, the degradation of MB is more for uniform cauliflower morphology of 4T and 6T compared to non-uniform shapes of 2T route prepared samples. The dye discoloration reaction that occurs on TiO_2 nanoparticles is due to the effective absorption of solar energy by the prepared titania catalysts and by reducing the electron-hole recombination. The fast degradation of MB occurs due to the effective absorption of solar energy and thus reduces the electron-hole recombination[24–25].

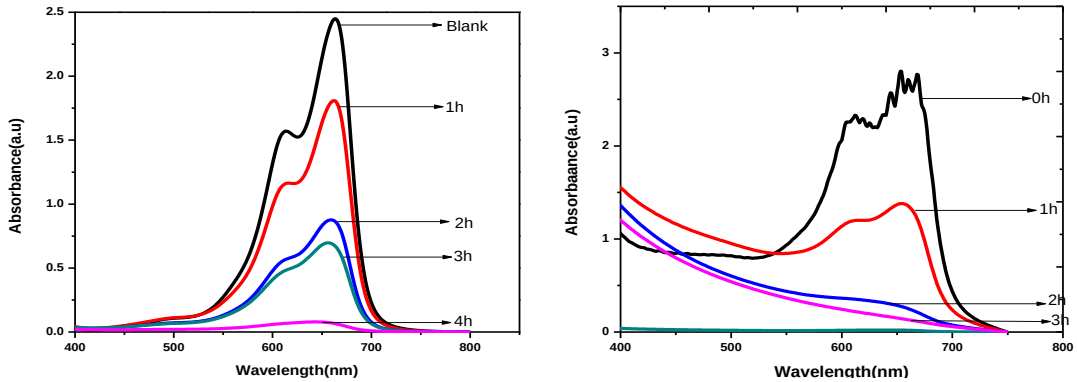

Fig. 6 (a-b) UV-Vis spectra of MB dye degradation at different time intervals at various Rutile Titania under visible light irradiation. (a) Reaction condition: P25-0.05g, MB-0.001g, Time-4h. (b) Reaction condition: 4T-0.05g, MB- 0.001g, Time-3h.

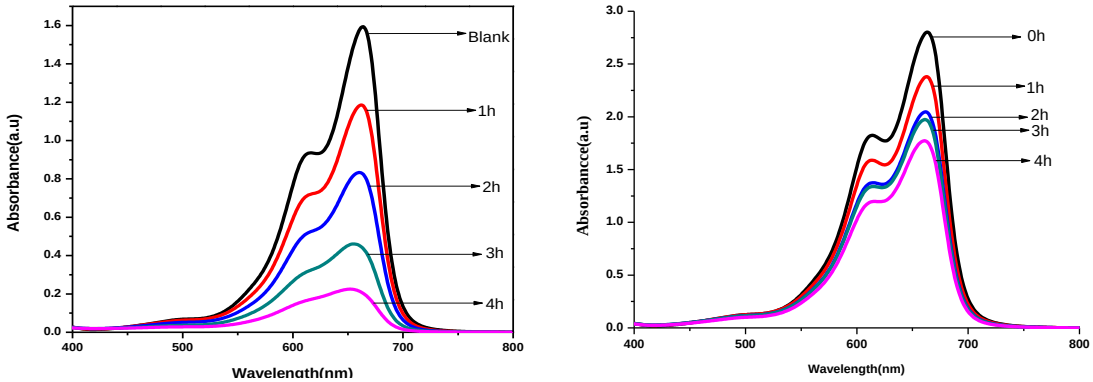

Fig. 7(a-b) UV-Vis spectra of MB dye degradation at different time intervals at various Rutile Titania under visible light irradiation. (a) Reaction condition: 6T-0.05g, MB- 0.001g, Time-4h. (bd) Reaction condition: 2T-0.05g, MB- 0.001g, Time-4h.

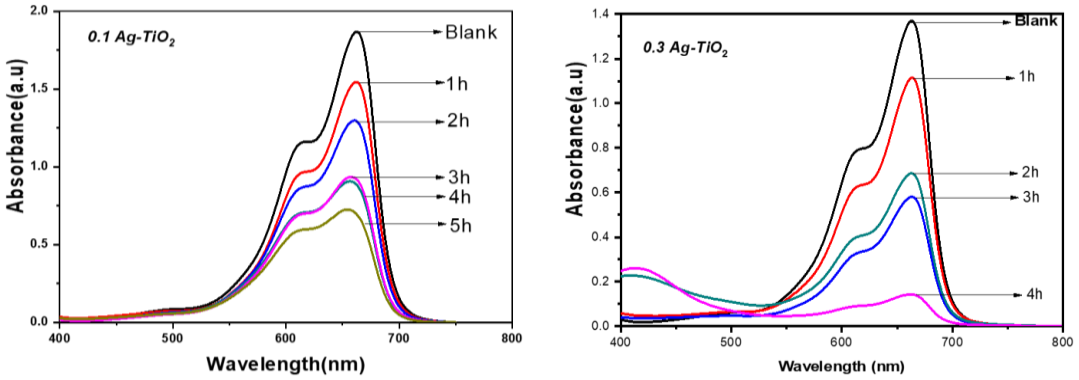

Fig. 8.1 (a,b) UV-Vis spectra of MB dye degradation at different time intervals at various Silver modified Rutile Titania under visible light irradiation.

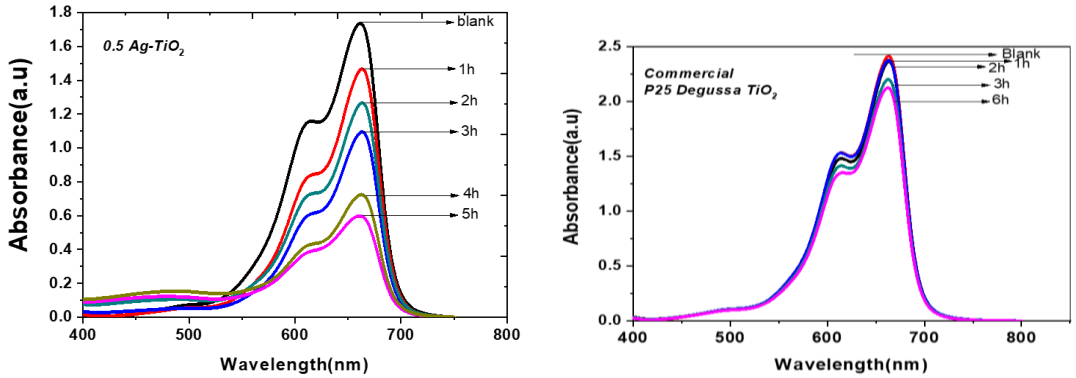

Fig. 8.2 (c,d) UV-Vis spectra of MB dye degradation at different time intervals at various Silver modified Rutile Titania under visible light irradiation.

It is observed that the degradation is more effective for the material with optimum concentration of silver nanoparticles incorporation (Fig.8). Methylene blue degradation occurs more effectively on in 0.3 AgT than 0.1 AgT and 0.5 AgT (Fig 8a-8d). This is because the photosensitive action of the materials under visible light increases when the Ag gets doped into the materials since it can shift the absorption edge of the materials to the visible region than undoped Titania materials. At the same time, the dye degradation is slightly decreased higher incorporation of silver particles in the lattice of titania. Lage particle formation by incorporation of a more weight ratio of silver in pristine rutile phase of titania causes the reduction in the catalytic active sites formation and hindrances in dye molecules sorption on the surface of silver modified titania. Hence, the optimized addition of silver NPs could provide effective results for photosensitive catalytic applications.

The degradation of MB occurs by the reaction of electrons and holes generated by the photosensitive materials with reaction solution after visible light irradiation. The fast degradation of MB occurs on 0.3AgT is due to the effective absorption of light energy and thus reduces the electron-hole recombination. This will enhance the photosensitive activity of the prepared materials. The observed reduction in MB concentration under visible light in the presence of prepared materials confirms the photosensitive activity of the TiO_2 based materials. Table 3 shows the effect of silver-modified catalyst weight on the conversion of dye degradation and discoloration efficiency. The optimized amount (500 mg) of silver incorporated titania catalyst showed the highest degradation percentage of 89%. A slight decreasing in catalyst weight (0.3Ag-TiO_2) decreases the degradation efficiency. The dye degradation efficiency follows the order such as 0.3Ag-TiO_2 > 0.5Ag-TiO_2 > 0.1Ag-TiO_2.

Table 3. Effect of silver modified catalyst weight on dye degradation efficiency.

SL.NO	SAMPLE	WEIGHT (g)	MB DEGRADATION (%)
1	P-25	0.05	10.2
2	TiO_2 (4T)	0.05	74.4
3	0.1 AgT	0.05	51.0
4	0.3 AgT	0.05 0.03 0.07	89.5 67.7 52.2
5	0.5 AgT	0.05	65.5
6	BLANK	0.05	21.5

The mechanism insights of direct visible light (sunlight) irradiation with various acid concentration methods prepared rutile titania was purly depend on surface area particle size

formation. In the present case, rutile phase of TiO_2 prepared with optimized acid condition found by the performance of 4T and 6T(4 M and 6 M) HNO_3 route prepared catalysts. The abvove catalyst only shows efficiently enrich the presence of surface-bound OH- species in the surface of cauliflower-shaped titania particles [29]. Increased surface active sites on a flower-like morphology enhance electron-hole recombination rate and possess a higher efficiency. The optimized concentration of 4 T and 6 T HNO_3 route prepared rutile titania was completely degrading the dye degradation. The photosensitive response of TiO_2 is represented in Fig. 7, which shows the production of OH radicals and O_2^- and the reaction of these species with the organic dye pollutants followed by the release of side products such as harmless organics, carbon dioxide, and water molecules.

4. Conclusion

Owing to the simplicity and feasibility of the process was achieved by acid assisted sol-gel process towards the synthesis of pure Rutile Titania and silver modified Titania with a mixed phase of rutile and anatase phase interference. XRD, SEM, and HR-TEM images confirm spherical shapes, cauliflower-shaped morphology formation, and in this case Ag-TiO_2 shows the hexagonal cubic rods formation. The specific surface area and cauliflower-like morphology further appreciate the improved photo light sensitivity and catalytic active cites generation in the surface of the structure of Titania. The as-prepared 4T and 6 T Rutile TiO_2 and 0.3 Ag-TiO_2 show efficient solar light harvesting ability for the higher degradation of methylene blue dyes. The enhanced photosensitivity was obtained due to tailored morphology TiO_2 and enriched surface active sites due to the acid treatment process in the hydrothermal method. In the future, as prepared rutile TiO_2 and silver modified titania could be utilized in photochromic film and sensitized solar cell applications.

Acknowledgments

The author (Fatimah Mohammed Alzahrani) greatful and the research was funded by Princess Nourah bint Abdulrahman University Researchers Supporting Project Number (PNURSP2022R42), Princess Nourah bint Abdulrahman University, Riyadh, Saudi Arabia. Also the author (khamael M. Abualnaja) greatful and thanks to Taif University Researchers Supporting Project number (TURSP-2020/267), Taif University, Taif, Saudi Arabia.

References

[1] R. Su, M. Christensen, Y. Shen, J. Kibsgaard, B. Elgh, R. T. Vang, R. Bechstein, S. Wendt, A. Palmqvist, B. B. Iversen, F. Besenbacher, J. Phys. Chem. C. 117, 27039 (2013); https://doi.org/10.1021/jp4106713

[2] G. Veréb, L. Manczinger, G. Bozsó, A. Sienkiewicz, L. Forró, K. Mogyorósi, K. Hernádi, A. Dombi, Appl. Catal. B Environ. 129, 566 (2013); https://doi.org/10.1016/j.apcatb.2012.09.045

[3] R. Jothi Ramalingam, T. Radhika, P. Reshma Ranjan, S. R. M. Sayed, H. A. Al-lohedan, A. Meera Moydeen, D. M. Al-dhayan, Int. J. Hydrogen Energy. 44, 23959 (2019); https://doi.org/10.1016/j.ijhydene.2019.07.117

[4] K. R. Anju, R. Thankapan, J. R. Rajabathar, H. A. Al-Lohedan, Optik 165, 408 (2018); https://doi.org/10.1016/j.ijleo.2018.03.091

[5] R. Jothi Ramalingam, A. K. Shukla, K. Kombaiah, J. J. Vijaya, A. M. Tawfeek, Optik 148, 325 (2017); https://doi.org/10.1016/j.ijleo.2017.08.129

[6] P. Latha, K. Prakash, S. Karuthapandian, Optik 154, 242 (2018);

https://doi.org/10.1016/j.ijleo.2017.10.054
[7] E. P. Da Silva, A. F. Rubira, O. P. Ferreira, R. Silva, E. C. Muniz, J. Colloid Interface Sci. 555, 373 (2019); https://doi.org/10.1016/j.jcis.2019.07.064
[8] X. Lin, M. Sun, B. Gao, W. Ding, Z. Zhang, S. Anandan, A. Umar, J. Alloys Compd. 850, 156653 (2021); https://doi.org/10.1016/j.jallcom.2020.156653
[9] J. George, C. C. Gopalakrishnan, P. K. Manikuttan, K. Mukesh, S. Sreenish, Powder Technol. 377, 269 (2021); https://doi.org/10.1016/j.powtec.2020.08.050
[10] N. N. Tri, D. Q. Ho, A. J. P. Carvalho, M. T. Nguyen, N. T. Trung, Surf. Sci. 703, 121723 (2021); https://doi.org/10.1016/j.susc.2020.121723
[11] A. Balapure, R. Ganesan, J. Colloid Interface Sci. 581, 205 (2021); https://doi.org/10.1016/j.jcis.2020.07.096
[12] K. Kumari, R. R. D.S. Arun Kumar, S. Meti, M. R. Rahman, Phys. B Condens. Matter. 597, 412386 (2020); https://doi.org/10.1016/j.physb.2020.412386
[13] R. Kumar, R. M. El-Shishtawy, M. A. Barakat, Catalysts, 6 (2016); https://doi.org/10.3390/catal6060076
[14] N. K. A. Hamed, M. K. Ahmad, N. H. H. Hairom, A. B. Faridah, M. H. Mamat, A. Mohamed, A. B. Suriani, N. Nafarizal, F. I. M. Fazli, S. M. Mokhtar, W. I. W. Omar, M. Shimomura, Appl. Surf. Sci. 534, 147571 (2020); https://doi.org/10.1016/j.apsusc.2020.147571
[15] H. Suzuki, K. Awa, S. ichi Naya, H. Tada, Catal. Commun. 147, 106148 (2020); https://doi.org/10.1016/j.catcom.2020.106148
[16] R. Jothi Ramalingam, T. Radhika, P. Reshma Ranjan, S. R. M. Sayed, H. A. Al-lohedan, A. Meera Moydeen, D. M. Al-dhayan, PInt. J. Hydrogen Energy. 44, 23959 (2019); https://doi.org/10.1016/j.ijhydene.2019.07.117
[17] I. Morad, A. M. Alshehri, A. F. Mansour, M. H. Wasfy, M. M. El-Desoky, Phys. B Condens. Matter., 597 (2020); https://doi.org/10.1016/j.physb.2020.412415
[18] Y. Lin, Z. Jiang, C. Zhu, R. Zhang, X. Hu, X. Zhang, H. Zhu, S. H. Lin, Int. J. Hydrogen Energy. 42, 4966 (2017); https://doi.org/10.1016/j.ijhydene.2016.06.077
[19] Y. Wan, B. Sun, W. Liu, C. Qi, J. Sol-Gel Sci. Technol. 61, 558 (2012); https://doi.org/10.1007/s10971-011-2659-5
[20] D. S. Mousavi, P. Asen, S. Shahrokhian, A. Irajizad, J. Colloid Interface Sci. 563, 241 (2020); https://doi.org/10.1016/j.jcis.2019.12.080
[21] A. Tiwari, A. Shukla, S. S. Choi, S.-M. Lee, Korean J. Chem. Eng. 35, 2133 (2018). https://doi.org/10.1007/s11814-018-0114-9
[22] H.-G. Park, J.I. Kim, M. Kang, M.-K. Yeo, Mol. Cell. Toxicol. 10, 293 (2014); https://doi.org/10.1007/s13273-014-0033-8
[23] L. Guo, K. Zhang, X. Han, Q. Zhao, D. Wang, F. Fu, Y. Liang, J. Alloys Compd., 816 (2020); https://doi.org/10.1016/j.jallcom.2019.152560
[24] R. Djellabi, M.F. Ghorab, G. Cerrato, S. Morandi, S. Gatto, V. Oldani, A. Di Michele, C. L. Bianchi, J. Photochem. Photobiol. A Chem., (2015).
[25] S. S. F. Carvalho, N. M. F. Carvalho, Inorg. Chem. Commun., 108 (2019); https://doi.org/10.1016/j.inoche.2019.107507
[26] S. A. Idrees, M. K. Ibrahim, ICOASE 2018 - Int. Conf. Adv. Sci. Eng., 389 (2018).